Doherty Load Modulation Based on Non-Reciprocity

Citation for the original published paper (version of record):
Saad, P., Zhou, H., Perez-Cisneros, J. et al (2021). Doherty Load Modulation Based on Non-Reciprocity. 2021 51st European Microwave Conference, EuMC 2021: 938-941. http://dx.doi.org/10.23919/EuMC50147.2022.9784157

Doherty Load Modulation Based on Non-Reciprocity

Paul Saad[#1], Han Zhou[*2], Jose-Ramon Perez-Cisneros[*3], Rui Hou[#4], Christian Fager[*5], Bo Berglund[#6]

[#]Ericsson AB, 164 80 Stockholm, Sweden

[*]Chalmers University of Technology, 412 96 Gothenburg, Sweden

{[1]paul.saad, [4]rui.hou,[6]bo.g.berglund}@ericsson.com, {[2]han.zhou, [3]jospere,[5]christian.fager}@chalmers.se

***Abstract* — This paper presents a new type of Doherty power amplifiers (DPA) based on non-reciprocal power combiners. We replace the conventional quarter-wave ($\lambda/4$) impedance inverter in a DPA by a non-reciprocal gyrator. As proof of concept, a DPA using a commercial circulator has been implemented. The prototype PA exhibits a peak output power of 49.1 ± 0.1 dBm and efficiency between 57-68 % at 6 dB output back-off (OBO) across 2.08 -2.14 GHz. Linearized modulated measurements, using 10 MHz LTE signal with 7.8 dB PAPR, show an average output power of 13 W, an average drain efficiency of 54 %, and an adjacent channel leakage ratio (ACLR) lower than -55 dBc.**

***Keywords* — Circulator, Doherty, energy efficiency, GaN-HEMT, power amplifiers.**

I. Introduction

Modern wireless communication systems, such as the 5^{th} generation (5G) mobile networks, achieve high spectral efficiency by multi-carrier techniques, such as orthogonal frequency-division multiplexing (OFDM) and high-order modulations such as 256 quadrature amplitude modulation (QAM). Such waveforms have high peak-to-average ratios (PAPR). The energy efficiency of such systems is determined by the average power levels significantly backed-off from the peak envelop power. For this reason, modern radio base-stations employ Doherty PAs for RF power amplification.

Besides the conventional Doherty combiner based on $\lambda/4$ transmission lines (TLs) [1], different types of Doherty combiners have been proposed throughout the years. Doherty load modulation can be achieved by a series connected load [2], by lumped elements based combiners when integration comes into play [3]–[5], and by multi-section distributed networks for bandwidth extension [6]–[10]. In this work, we propose a new Doherty combiner based on non-reciprocity. It is obtained by substituting the conventional impedance inverter network (IIN) with a ferromagnetic gyrator. As it will be demonstrated, the classic Doherty load modulation can be achieved by the proposed technique.

This paper is organized as follows. The proposed architecture is explained in Section II. Then, the prototype implementation is presented Section III, the experimental results are shown in Section IV, and conclusions are given in Section V.

II. Theory of Operation

The operating principle of a conventional DPA (Fig. 1(a)) has been abundantly described in literature so we simply refer

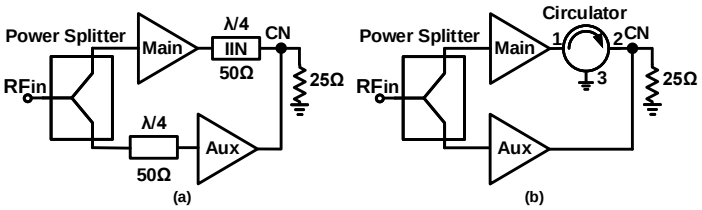

Figure 1. Block diagrams. (a) conventional DPA. (b) proposed architecture.

to the classic texts (e.g. in [11]). By definition, the $\lambda/4$ inverter has the following S-parameters matrix

$$[S] = \begin{bmatrix} 0 & -j \\ -j & 0 \end{bmatrix} \tag{1}$$

In contrast, in the proposed technique presented in Fig. 1 (b), we

1) replace the $\lambda/4$ inverter by a *gyrator*, and
2) remove the $\lambda/4$ phase compensation in front of the auxiliary amplifier.

An ideal gyrator is a linear, passive, lossless two-port electrical network element [12], defined by the S-parameters

$$[S] = \begin{bmatrix} 0 & -1 \\ 1 & 0 \end{bmatrix} \tag{2}$$

Since $S_{12} \neq S_{21}$, a gyrator is non-reciprocal. Microwave gyrators existed since the 1950s based on Faraday rotations in ferromagnetic materials [13]. For availability, without losing generality, we use a microwave circulator to demonstrate the principle in this work. It is trivial to show that an ideal circulator

$$[S] = \begin{bmatrix} 0 & 0 & 1 \\ 1 & 0 & 0 \\ 0 & 1 & 0 \end{bmatrix}$$

with its 3^{rd} port short-terminated (shown in Fig. 1(b)), degenerates into a two-port that is identical to (2), i.e. a gyrator. (Proof: $S_{12,gyrator} = S_{13,circ} S_{32,circ} \Gamma_{short} = -1$).

We then demonstrate that Fig. 1(b) behaves exactly the same as Fig. 1(a), i.e. a conventional DPA. Firstly, at power back off, the auxiliary amplifier is turned off. The main amplifier sees a reflection coefficient at its intrinsic plane

$$\Gamma_{main} = S_{12} S_{21} \Gamma_{25\,\Omega}, \tag{3}$$

which, according to either (1) or (2), equals to 1/3 ($100\,\Omega$). Secondly, at peak power level, both the main and auxiliary amplifiers see a $50\,\Omega$ load without reflections. In this case,

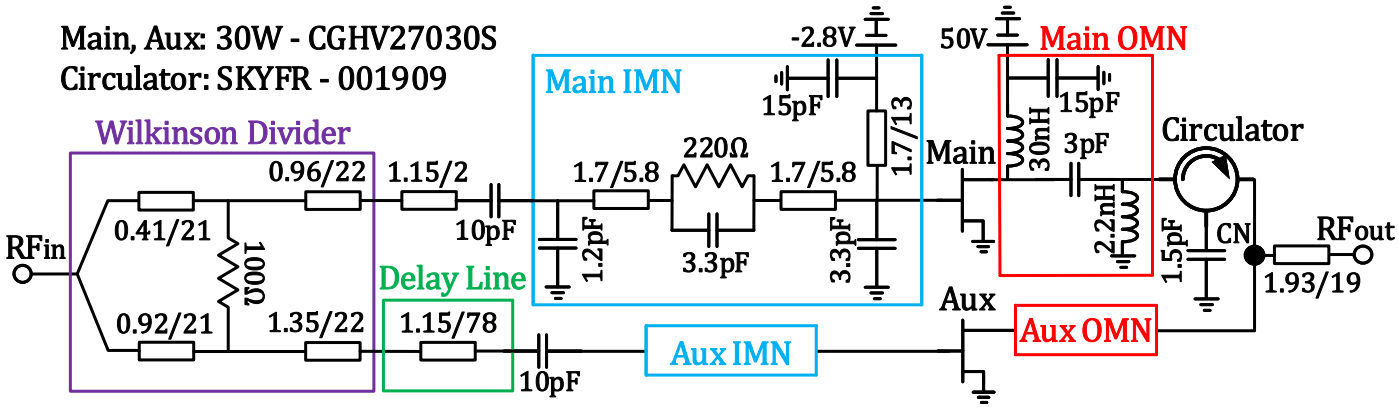

Figure 2. Schematic of the Doherty PA implemented on a Rogers $4003C$ substrate with $\varepsilon_r = 3.55$ and a thickness of 0.52 mm. "/" refers refers to width/length in millimeters.

the only difference is the phase of S_{21} (90° delayed by an inverter (1) and 0° delayed by a gyrator (2)). For this reason, a conventional DPA employs a 90° TL at the input of the auxiliary amplifier to enforce in-phase power combining at the combining node. This 90° phase compensation is removed in Fig. 1(b) to enforce the same in-phase power combining. Fig. 1(a) and (b) perform exactly the same Doherty load modulation at power back-off and the same in-phase power combining at the peak power level.

III. Prototype Design and Implementation

To demonstrate the newly proposed architecture, a 60 W PA operating at 2.11 GHz has been designed. The 30 W GaN-HEMT device, CGHV27030S, is used for the main and auxiliary amplifiers. The device operates at 50 V drain voltage and has a saturation drain current of 2.6 A. The circuit diagram of the designed DPA is shown in Fig. 2 where all the dimensions and component values are given.

At the input, an uneven Wilkinson splitter [14] is used to ensure proper turn-on condition for the auxiliary device biased in Class-C. Consequently, 40 % of the input power goes to the main amplifier and 60 % is directed towards the auxiliary amplifier. The input matching networks (IMNs) for the main and auxiliary amplifiers are identical two-stage low-pass networks, including a parallel $R-C$ stabilization networks to ensure unconditional stability conditions. They are constituted of a mixture of distributed TLs and lumped components, as shown in Fig. 2. Identical narrowband output matching networks (OMNs) are used for the main and auxiliary amplifiers. Each OMN consists of a series capacitor and shunt inductor. Their values are selected, respectively, to resonate the drain bondwire inductance and the drain-source capacitance at 2.11 GHz. A commercial three-port surface mount circulator from Skyworks, $SKYFR-001909$, having its third port shorted through a capacitor, is used as an IIN. A $\lambda/4$ TL is used to transform the 25 Ω output impedance of the DPA at the common node to 50 Ω. Finally, a delay line has been added at the input of the auxiliary IMN to compensate for the phase shift introduced by the circulator and, hence, to ensure in phase power combining at the connecting node.

The simulated intrinsic current, voltage, and load impedance profiles are presented in Fig. 3. As it can be noticed, they exhibit the same behavior as a conventional DPA. The main transistor outputs a drain current proportional to its input voltage. The auxiliary, switched off below the OBO level, ramp

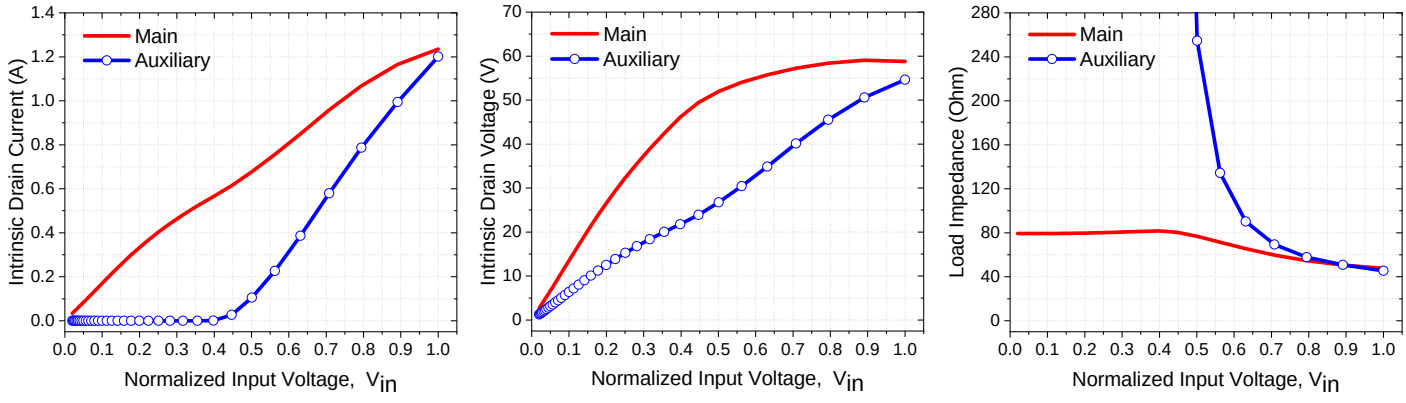

(a) (b) (c)

Figure 3. Simulated intrinsic characteristics of the main and auxiliary amplifiers (a) current, (b) voltage, and (c) load impedance.

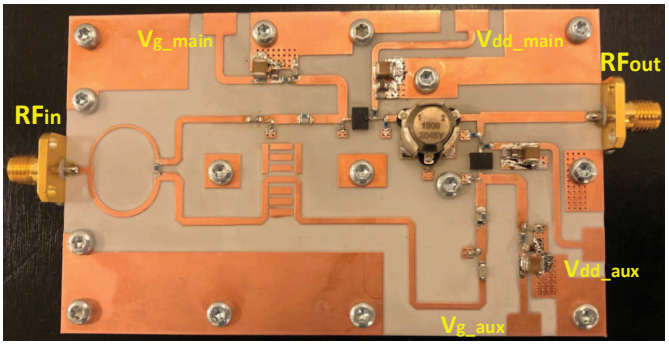

Figure 4. Photo of the implemented Doherty power amplifier.

up to achieve, together with the main, their maximum currents at the maximum input voltage. When the auxiliary is turned on at the OBO level, the voltage across the main becomes constant, as shown Fig. 3(b), and the main starts to behave as a voltage source. Furthermore, the load impedances of the main and auxiliary amplifiers decrease respectively from 80 Ω and ∞ to reach their R_{opt} at the maximum input voltage.

Fig. 4 shows a photo of the prototype PA. It has been implemented on a Rogers $4003C$ substrate with $\varepsilon_r = 3.55$ and thickness of 0.52 mm. Its size is $10 \times 6\,cm^2$.

IV. Measurement Results

The PA has been characterized by small-signal, large-signal, and modulated signal measurements to evaluate its performance.

A. Small-Signal Measurements

The realized DPA was measured in small-signal conditions to study its frequency response. A drain bias of 50 V was used for the main and auxiliary devices. The main amplifier was biased for a quiescent drain current of 40 mA while the auxiliary amplifier was biased in class-C. The S-parameters, presented in Fig. 5, show a fairly good agreement between simulation and measurements. Across 2.08-2.14 GHz, the small-signal gain (S21) is 16-17.5 dB and the input return loss, (S11), is better than 12 dB.

B. Large-Signal Measurements

Using similar bias conditions as above, pulsed continuous wave (CW) signals of 10 us pulse width and 10% duty cycle have been employed to realize the large-signal measurements. Fig. 6 shows the power gain and drain efficiency for all frequencies within 2.08-2.14 GHz. The measured peak output power is 49.1 ± 0.1 dBm and the corresponding power gain and drain efficiency are 13.5-14 dB and 69-73 %, respectively. At 6 dB OBO, corresponding to 43.1 ± 0.1 dBm output power, the measured power gain and drain efficiency are 14.7-15 dB and 57-68 %, respectively. It is evident that, Doherty-like, high efficiency enhancement is obtained at 6 dB OBO.

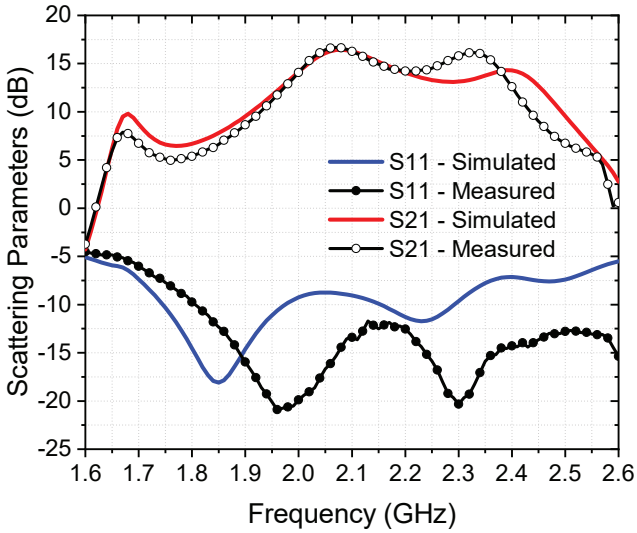

Figure 5. Measured and simulated S-parameters of the realized Doherty power amplifier.

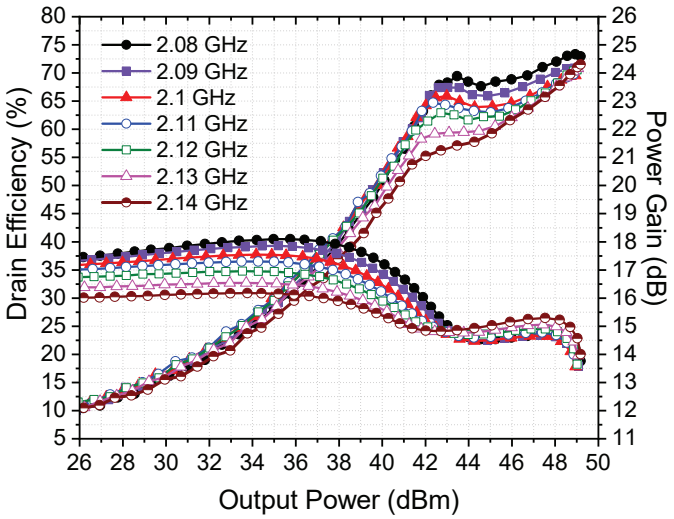

Figure 6. Measured drain efficiency and gain vs. output power at different frequencies.

C. Modulated Measurements

An 8-tap finite impulse response (FIR) equalizer, with magnitude dependent coefficients from look-up tables (LUTs), is used for the DPD. Among the 8 LUTs, 6 of them contain diagonal terms and the other 2, off-diagonal terms [15]. Each LUT has 64 equally-spaced entries and linear interpolation in between the entries [16]. The sampling rate of the DPD is 184.32 MS/s for the single-carrier case. The experimental linearization setup employs a Rohde & Schwarz SMW200A signal generator and a Rohde & Schwarz FSW43 spectrum analyzer.

The characterization of the PA with a modulated signal considers an LTE signal of 10 MHz bandwidth, 7.8 dB PAPR, at 2.11 GHz. The measured output spectrum, before and after DPD, is presented in Fig. 7. Average output power, average drain efficiency, and ACLR, with and without DPD are

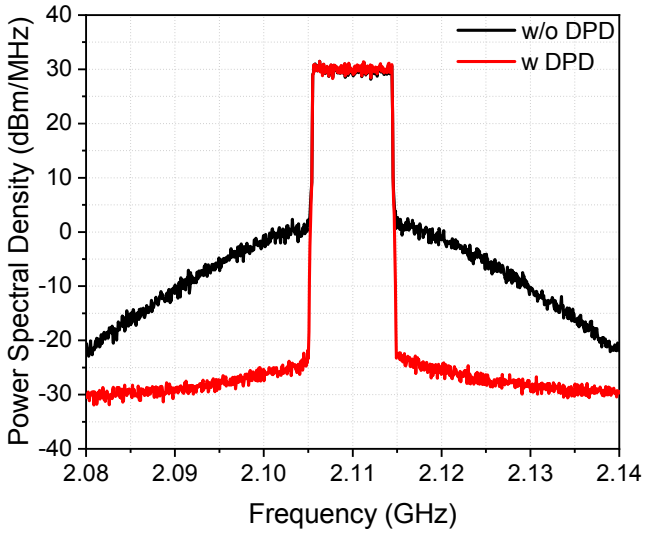

Figure 7. PA output signal spectrum of 10 MHz LTE signal with and without digital predistortion.

Table 1. Average output power, average drain efficiency, and ACLR.

Scenario	$Pout$(dBm)	η(%)	ACLR(dBc) w/o DPD	ACLR(dBc) w DPD
@2.11 GHz				
10MHz LTE	41.1	54	$-31.6/-31$	$-56.1/-55$

"/" refers to lower/upper adjacent channels.

summarized in Table 1. For an average output power of 13 W, the ACLR level is lower than -55 dBc at an average drain efficiency of 54 %.

Table 2 confirms that the proposed DPA shows competitive performance when compared to the best conventional DPAs in the literature.

V. Conclusion

A new DPA architecture has been proposed by substituting the quarter-wave impedance inverter of a DPA with a ferromagnetic gyrator, exemplified by a short-terminated circulator. As a proof of concept, a DPA using a circulator has been designed at 2.11 GHz. The evaluation of the DPA showed a peak output power of 49.1 dBm and a Doherty-like efficiency profile with 65 % drain efficiency at 6 dB OBO. Furthermore, modulated signal measurements demonstrated that the newly proposed architecture can be linearized to meet wireless communications systems standard with competitive performance.

Table 2. State-of-the-art conventional DPAs.

Reference	Freq(GHz)	$Pout_{sat}(dBm)$	$Gain_{sat}(dB)$	$\eta_{6dB}(\%)$
[17]	2.14	46	9	61
[18]	2.6	52.5	11	55
[19]	2.5	47	10	54
This work	**2.11**	**49.1**	**13.5**	**65**

Acknowledgment

The authors would like to thank Skyworks for providing the circulators for this experiment. We are also grateful to Ronny Carlsson from Skyworks for valuable technical discussions.

References

[1] F. H. Raab, "Efficiency of Doherty RF power-amplifier systems," *IEEE Trans. Broadcast.*, vol. BC-33, no. 3, pp. 77–83, Sep. 1987.

[2] S. Kawai, Y. Takayama, R. Ishikawa, and K. Honjo, "A GaN HEMT Doherty amplifier with a series connected load," *Proc. Asia-Pacific Microw. Conf.*, 2009, pp. 325–328.

[3] C. Tongchoi, M. Chongcheawchamnan, and A. Worapishet, "Lumped element based Doherty power amplifier topology in CMOS process," *IEEE Int. Circuits Syst. Symp. Dig.*, 2003, vol. 1, pp. I-445–I-448.

[4] D. Yu, Y. Kim, K. Han, J. Shin, and B. Kim, "Fully integrated Doherty power amplifiers for 5 GHz wireless-LANs," *IEEE MTT-S Radio Frequency Integr. Circuits Symp. Dig.*, 2006, pp. 177–180.

[5] M. Elmala, J. Paramesh, and K. Soumyanath, "A 90-nm CMOS Doherty power amplifier with minimum AM-PM distortion," *IEEE J.Solid-State Circuits*, vol. 41, no. 6, pp. 1323–1332, Jun. 2006.

[6] L. Piazzon, R. Giofre, P. Colantonio, and F. Giannini, "A wideband doherty architecture with 36% of fractional bandwidth," *IEEE Microw. Compon. Lett.*, vol. 23, no. 11, pp. 626–628, Nov. 2013.

[7] E. Bertran and M. Yahyavi, "A wideband doherty-like architecture using a klopfenstein taper for load modulation," *IEEE Microw. Compon. Lett.*, vol. 25, no. 11, pp. 760–762, Nov. 2015.

[8] A. Barakat, M. Thian, V. Fusco, S. Bulja, and L. Guan, "Toward a More Generalized Doherty Power Amplifier Design for Broadband Operation," *IEEE Trans. Microw. Theory Techn.*, vol. 65, no. 3, pp. 846–859, Mar. 2017.

[9] P. Saad, R. Hui, R. Hellberg, and B. Berglund, "Ultra-Wideband Doherty-Like Power Amplifier," *IEEE MTT-S Int. Microw. Symp. Dig.*, Philadelphia, PA, USA, Jun. 2018.

[10] P. Saad, R. Hui, R. Hellberg, and B. Berglund, "The Continuum of Load Modulation Ratio From Doherty to Traveling-Wave Amplifiers," *IEEE Trans. Microw. Theory Techn.*, vol. 67, no. 12, pp. 5101–5113, Dec. 2019.

[11] S. C. Cripps, "RF Power Amplifiers for Wireless Communications," *2nd ed. Norwood*, MA: Artech House, 2006.

[12] B. D. H. Tellegen, "The Gyrator, A New Electric Network Element," *Philips Res. Rep.*, vol. 3, no. 1, pp. 81–101, 1948.

[13] C. L. Hogan, "The ferromagnetic Faraday effect at microwave frequencies and its applications: The microwave gyrator," *The Bell Syst. tech.*, vol. 31, no. 1, pp. 1–31, Jan. 1952.

[14] E. Wilkinson, "An N-way hybrid power divider," *IRE Trans. Microw. Theory Techn.*, vol. 8, no. 1, pp. 116–118, Jan. 1960.

[15] D. R. Morgan, Z. Ma, J. Kim, M. G. Zierdt, and J. Pastalan, "A Generalized Memory Polynomial Model for Digital Predistortion of RF Power Amplifiers," *IEEE Trans. Signal Process.*, vol. 54, no. 10, pp. 3852–3860, Oct. 2006.

[16] A. Molina, K. Rajamani, and K. Azadet, "Digital Predistortion Using Lookup Tables With Linear Interpolation and Extrapolation: Direct Least Squares Coefficient Adaptation," *IEEE Trans. Microw. Theory Techn.*, vol. 65, no. 3, pp. 980–987, Mar. 2017.

[17] Y. Lee, M. Lee and Y. Jeong, "Highly Efficient Doherty Amplifier Based on Class-E Topology for WCDMA Applications," *IEEE Microw. Compon. Lett.*, vol. 18, no. 9, pp. 608–610, Sept. 2008.

[18] H. Deguchi, N. Ui, K. Ebihara, K. Inoue, N. Yoshimura and H. Takahashi, "A 33W GaN HEMT Doherty amplifier with 55% drain efficiency for 2.6GHz base stations," *IEEE MTT-S Int. Microw. Symp. Dig.*, Boston, MA, 2009, pp. 1273-1276.

[19] A. Z. Markos, K. Bathich, F. Golden and G. Boeck, "A 50 W unsymmetrical GaN Doherty amplifier for LTE applications," *The 40th European Microw. Conf.*, Paris, 2010, pp. 994-997.